MODEL STUDY OF SUPPORTED BIMETALLIC CATALYSTS

Zlatko KNOR and Jan ŠOTOLA

The J. Heyrovský Institute of Physical Chemistry and Electrochemistry, Czechoslovak Academy of Sciences, 182 23 Prague 8

Received November 11th, 1987
Accepted November 23rd, 1987

Dedicated to Dr R. Zahradník on the occasion of his 60th birthday.

Oxidized surface of a tungsten sample has been used as a carrier for palladium and/or molybdenum clusters, prepared by vacuum deposition. Field electron emission microscopy has been applied to study these sandwich systems (Pd, $Mo/WO_x/W$). In this work, nitrogen spill-over between neighbouring molybdenum and palladium clusters (islands) was demonstrated. The crystallographic orientation of these clusters has been studied by field ion microscopy.

Bimetallic systems are frequently used as heterogeneous catalysts for a variety of reactions, either as substitutes for more expensive single metal catalysts or because of some special properties (e.g. high selectivity, long life time). Prior to successful rational "tailor-making" of a new bimetallic (or multimetallic) catalysts one has to know the role of individual components in a particular catalytic reaction. For example, one can combine a metal which chemisorbs dissociatively reactant molecules (exhibiting zero reactivity of strongly bound chemisorbed species) and a metal (which does not chemisorb all kinds of reactant molecules) which is catalytically active, provided that the appropriate reactant fragments are supplied either from the gas phase[1] or by surface migration[2]. In these systems the trapping centers are spatially separated from the reaction sites. This, however, may be a quite common phenomenon in heterogeneous catalysis even on single metal catalysts, where the atomic steps or defects represent most probably the trapping centers[3] and the reaction (e.g. the recombination of various reactant fragments) might occur even on flat regions of the surface. The possibility of the existence of different trapping and reaction sites on a single metal catalyst has been experimentally demonstrated for the reaction of hydrogen with adsorbed oxygen on the vicinal regions around (111) plane of Pt and Ir[4]. These results also strongly supported the applicability of the Localized-Delocalized-Electrons Interplay (LDEI) model of the surface interactions on the transition-metal surfaces, based on the qualitative quantum chemical interpretation of FIM images[5,6]. In this model the role of trapping centers, screening effects and dissipation of excess kinetic energy of impinging gas molecules in the mechanism of the surface chemical interactions has been specified[7].

In the present work, we have chosen as a bimetallic catalyst a combination of a platinum-group metal (Pd, Ir) and tungsten (or molybdenum). The interaction of these systems with nitrogen (one reactant in the ammonia synthesis) has been studied in our laboratory. The most difficult step in the ammonia synthesis is believed to be the dissociation of nitrogen molecules[8]. In our system, tungsten (or molybdenum) represents the surface region for the dissociative trapping of nitrogen, whereas platinum group metals (which do not chemisorb nitrogen molecules at room temperature, c.f. ref.[2] and quotations therein) might serve as a reaction zone, being good hydrogenation catalysts. However, two conditions have to be fulfilled: (i) nitrogen atoms must be able to migrate from the trapping sites towards the reaction zone and (ii) their reactivity there must be proved. At room temperature, both the spill-over of nitrogen atoms in the palladium–tungsten system[2] and the hydrogenation of nitrogen atoms (deposited from the gas phase onto the iridium surface)[1] has been demonstrated in our Laboratory.

EXPERIMENTAL

Field emission microscopy (both field electron emission microscopy — FEM and field ion microscopy — FIM)[9,10] have been used throughout our study. The area of the sample surface imaged in these microscopes (the apex of the sharp tip, centrally projected by electrons or ions onto the fluorescent screen with the magnification of about 10^6 and resolution — FEM: 2 nm, FIM: 0·3 nm) has the size within the range of sizes of metal particles in the commercial supported metal catalysts (approximately tens of nanometers[11,12]). However, the small single crystal which forms the apex of the tip is in a direct contact with the bulk of the metallic wire from which the tip is prepared. Thus its properties might differ from those of metallic particles on an oxide carrier. Since it is difficult to work in the field emission microscopes with tips, prepared from oxides, we had to use as a carrier a thick oxide layer, prepared "in situ" by heavy oxidation of the tungsten tip (FEM: $p(O_2) \approx 10^{-4}$ Pa, exposure 240 s at $T \approx 300$ K, last 30 s at $T \approx$ $\approx 1\,100$ K; FIM: $p(O_2) \approx 10^{-3}$ Pa, exposure 240 s at $T \approx 300$ K, last 20 s at $T \approx 1\,100$ K — shorter heating time in FIM was needed to preserve the tip sharper than in FEM; shorter time being ,,compensated" by higher pressure of oxygen). An all-glass UHV apparatus (Fig. 1)

FIG. 1

Scheme of the apparatus: MP_i mechanical roughing pumps; DP oil diffusion pumps (DP-1 filled with Convalex, DP-2 and DP-3 filled with DC-705); TP turbomolecular pump; GIP getter ion pump; SP_i sorption pumps (mechanical mixture of zeolite 13X and of active charcoal, cooled by liquid nitrogen); TiSP titanium sublimation pump; FEM field electron (emission) microscope; FIM field ion microscope; T_i traps, cooled by liquid nitrogen; WB watercooled baffle; V_i greased glass valves (Apiezon N); GV_i ground-glass valves; LV leak valve; M_i bakeable metallic valves; T_i gas reservoirs; EV expansion volume; BAG_i Bayard–Alpert ionization gauges; IG classical ion gauge; TG_i thermocouple gauges, Ω omegatron mass spectrometer; a—k are the heating tapes ($T \approx 470$ K); A—D are ovens for baking out the principal parts of the apparatus ($T \approx 670$ K) (with the exception of D which can be heated to 470 K only, because of the presence of the channel-plate image intensifier in FIM). I FEM apparatus, II FIM apparatus, III gas handling

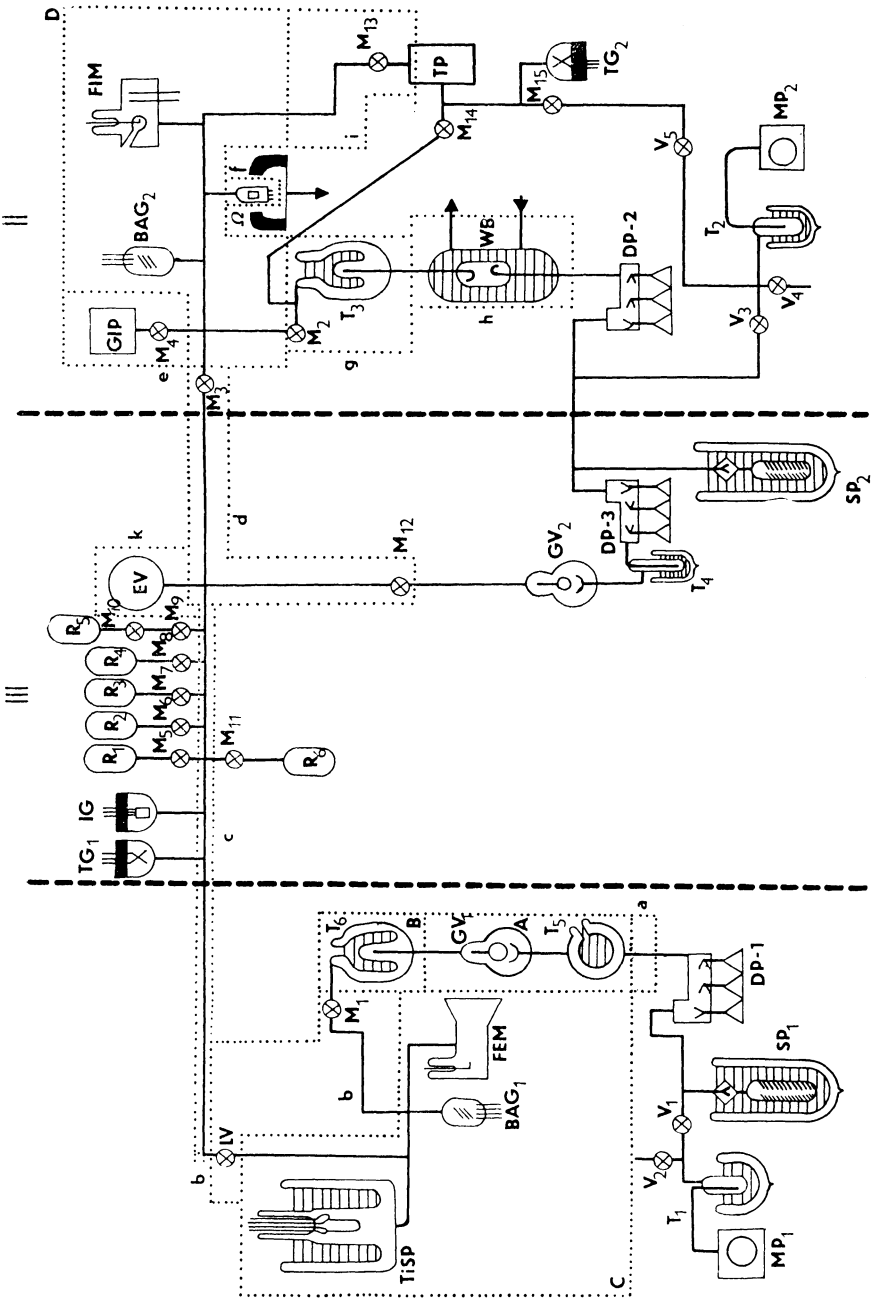
D
FIM
M13
TP
TG2
M15
M14
MP2
V5
BAG2
WB
DP-2
T2
V4
V3
GIP
M4
M2
T3
M3
SP2
DP-3
T4
GV2
M12
EV
k
d
R5
R4
R3
R2
R1
M10
M9
M8
M7
M6
M5
M11
R6
IG
TG1
c
T6
B
GV1
A
T5
a
DP-1
M1
FEM
SP1
b
BAG1
V1
LV
V2
T1
TiSP
MP1
C
II
III

has been used in these experiments. Base pressures of residual gases in FEM (Fig. 2) were $p \approx 4 . 10^{-8}$ Pa, pressures during palladium deposition were $p \leq 1 . 10^{-7}$ Pa and during the deposition of molybdenum $p \leq 5 . 10^{-7}$ Pa. Base pressures of residual gases in FIM (Fig. 3) were slightly higher ($p \approx 2 . 10^{-6}$ Pa), because the FIM part of the apparatus has to be outgassed at maximum $T \approx 470$ K (since the channel-plate image intensifier, used there, would lose its sensitivity at higher temperatures), whereas other parts of the apparatus have been frequently outgassed at $T \approx 670$ K. However, no serious contamination was detected even if the high electric field has been switched off for a time period of 300 s and even when the imaging gas has been changed (see Fig. 4). Palladium has been deposited onto the oxide layer in FIM in presence of the imaging gas (p(Ne) $\approx 1 . 10^{-3}$ Pa).

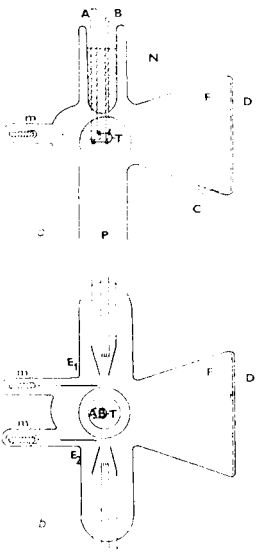

FIG. 2

Scheme of field electron emission microscope FEM (a side view (*a*) and a top view (*b*)): T the sample (a sharp tip); A the holder of the loop to which the tip is spotwelded; B additional contacts for resistance measurement of the temperature of the central part of the loop; N liquid nitrogen reservoir; F fluorescent screen; C external contact to the transparent electrode D; m magnetically operated shutters of the evaporation sources of Pd and Mo (E_i); P connection to the vacuum system

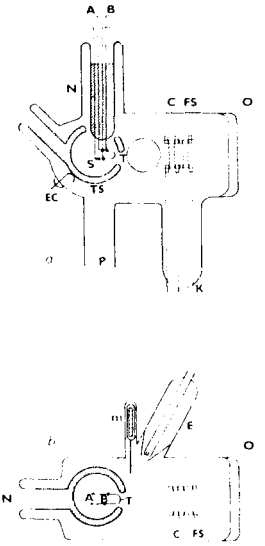

FIG. 3

Scheme of the field ion microscope FIM (a side view (*a*) and a top view (*b*)): T the sample (a sharp tip), spotwelded to the loop S; N liquid nitrogen; K external contact to the holder of the image intensifier (C channel-plate, FS fluorescent screen, covered with transparent electrode); EC external contact to the transparent electrode, covering the thermal shield TS; A and B have the same meaning as in Fig. 2)

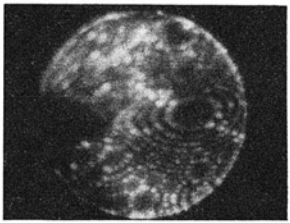

a

b

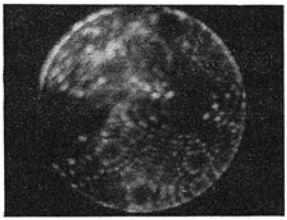

c

FIG. 4

Field ion image of a clean tungsten: *a* helium image (p(He) = 1·5 . 10^{-2} Pa) at 78 K, best image voltage (BIV) 3·9 kV; *b* imaging field switched off for 300 s and then again switched on: He, BIV = 3·9 kV, T = 78 K; *c* helium gas pumped down, neon image (p(Ne) = 1 . 10^{-2} Pa) BIV = 3·1 kV, T = 78 K

RESULTS AND DISCUSSION

Application of FIM *Technique*

Structural analysis of palladium layers deposited onto the WO_x surface has been attempted by means of FIM. Fig. 5 shows the sequence of images: *a* of a clean tungsten surface (well ordered atomic structure between (110) and (111) planes); *b* of the oxidized surface WO_x (random structure, where no definite conclusions can be made about the chemical quality of the imaged bright spots – which are most probably tungsten atoms in the oxide matrix[13–16]); *c* of palladium deposited over all surface at 78 K and heated afterwards for 5 s at about 1 100 K (random structure); *d* of the preceding layer after field evaporation of random upper layers (the exact number of evaporated layers could not be estimated with neon imaging gas) (a regular structure in the lower part of the image starts to be visible); e of the same system after continued field evaporation (a regular structure with tetragonal symmetry becomes visible in the lower part of the image, corresponding to the (111) region of the original tungsten surface, exhibiting hexagonal symmetry – compare Fig. 4 with Figs 5 and 6).

The average tip radius can be roughly estimated from the number of net planes between (110) and (112) planes[17]. Furthermore, the distance between the centers of (110) and (112) planes equals one half of the tip radius[18] and thus the real distances on the tip surfaces can be judged from FIM images. The distance between two tungsten atoms on the atomically rough (111) plane was $\approx$0·46 nm (estimated in the above mentioned way from Fig. 4) in good agreement with the theoretical value 0·45 nm (ref.[19]). The distance of edges of (100) planes in a (113) plane of palladium, estimated from Fig. 5e (compare the structure within the white circle and Fig. 6) is $\approx$0·43 nm. Theoretical value of this distance is 0·45 nm (the width of the step is 0·41 nm). The lattice constant of palladium was estimated from Fig. 5 (cf. Fig. 6) to be 0·38 nm (published value[19] is 0·39 nm). All these rough estimates were made under the assumption that the local radius of curvature of a palladium cluster (island) is not too much different from the average tip radius (no additional magnification of the palladium island occurs). Thus one can conclude that the observed palladium cluster, grown on the WO_x layer is oriented by a (100) plane parallel with the surface plane. This agrees well with the orientation of palladium whiskers, grown by high temperature–high field treatment directly on a clean tungsten substrate on the atomically flat (100) region[2].

Application of FEM *Technique*

In modeling supported metal catalysts in FEM we were facing two major problems, viz. whether the second metal will be visible (the oxidized tungsten surface exhibits very low electron emission) and whether it will rest solely upon the oxide layer or

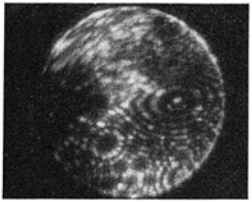

a

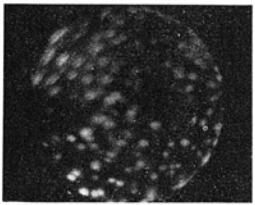

b

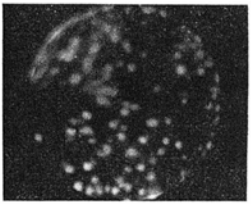

c

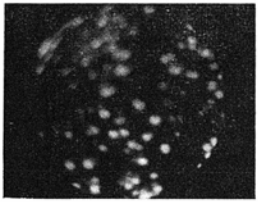

d

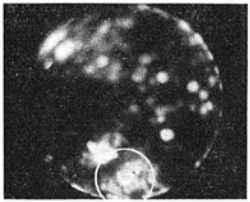

e

FIG. 5

Field ion images: *a* clean tungsten, helium image BIV = 3·9 kV, T = 78 K, field evaporation voltage (FEV) 4·3 kV; *b* oxidized tungsten surface, (for description of the oxidation procedure see text), neon image 78 K, FEV = BIV = 2·5 kV; *c* evaporated Pd layer at 78 K, subsequently heated for 5 s to about 1 100 K in the absence of the electric field, neon image, FEV = BIV = = 2·5 kV; *d* neon image, FEV = 3·4 kV, BIV = 2·5 kV, (the first regular structure appears in the lower part of the image — most probably a Pd cluster); e neon image, FEV = 4·1 kV, BIV = = 2·5 kV (Pd cluster with tetragonal symmetry in the lower part of the image (compare with Fig. 6)

directly contact the underlaying tungsten (in the case of free holes in the oxide layer). The former problem is positively solved in Fig. 7, where both palladium and molybdenum are proved to be visible, when deposited onto the oxide layer WO_x, prepared "in situ" on a tungsten tip. A direct lateral contact of the second metal (palladium) via a hole in the oxide layer with the underlaying material of the FEM tip (tungsten) can be excluded on the basis of experiments with nitrogen. Palladium does not chemisorb nitrogen molecules at room temperature[2]. Thus the absence of any change of the palladium work function (estimated from the Fowler–Nordheim plot)[10] in the $Pd/WO_x/W$ system (where the electron emission from palladium only is observed, see Fig. 7) rules out a lateral contact between Pd and W which would otherwise enable the spill-over of nitrogen atoms from tungsten towards palladium surface[2]. The absence of a direct vertical contact of Pd with W has been confirmed by application of higher temperatures (1 300–2 300 K) onto these composite systems. At these temperatures palladium, deposited on a part of clean tungsten, spreads over all the tip surface, evaporates and forms alloys with it[2], whereas on WO_x layers palladium coalesces and evaporates (Fig. 8).

The spill-over of nitrogen atoms from tungsten towards palladium surface was observed in a preceding paper[2]. In that case palladium has been deposited onto a clean tungsten and palladium microtip have been prepared by high temperature--high field treatment of the Pd–W system. The end radius of such palladium microtip was considerably smaller than the average radius of curvature of the original tungsten tip. Thus at a given voltage the field in the vicinity of the Pd surface was much higher then at the tungsten surface and consequently the electron emission from tungsten could be kept negligibly small in comparison with the emission from the Pd microtip. The work function changes (WFC's) of palladium could thus be selectively estimated from the Fowler–Nordheim plot. In the case of supported bimetallic system (Pd–Mo, deposited on the WO_x layer) the difference between the average work functions

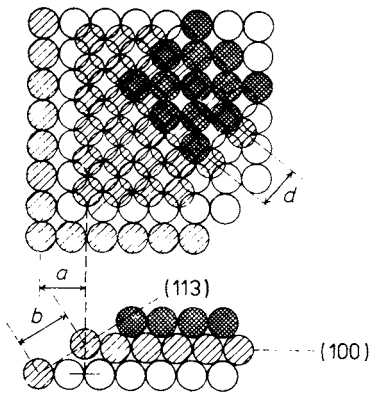

FIG. 6
Schematic view of steps around the (100) plane of the FCC lattice

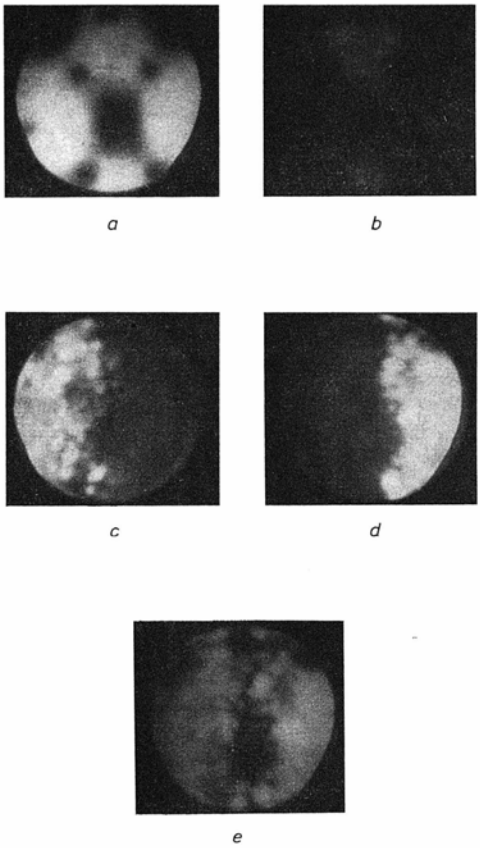

FIG. 7

Field electron emission images: *a* clean tungsten (imagir.g voltage $V = 3$ kV, $T = 78$ K); *b* oxidized surface (for description of the oxidation procedure see text) (image: $V = 4{\cdot}1$ kV, $T = 78$ K); *c* molybdenum deposited from the left side ($V = 4{\cdot}1$ kV, $T = 78$ K) *d* palladium deposited from the right side ($V = 4{\cdot}1$ kV, $T = 78$ K); *e* molybdenum evaporated onto *d* from the left side ($V = 4{\cdot}1$ kV, $T = 78$ K)

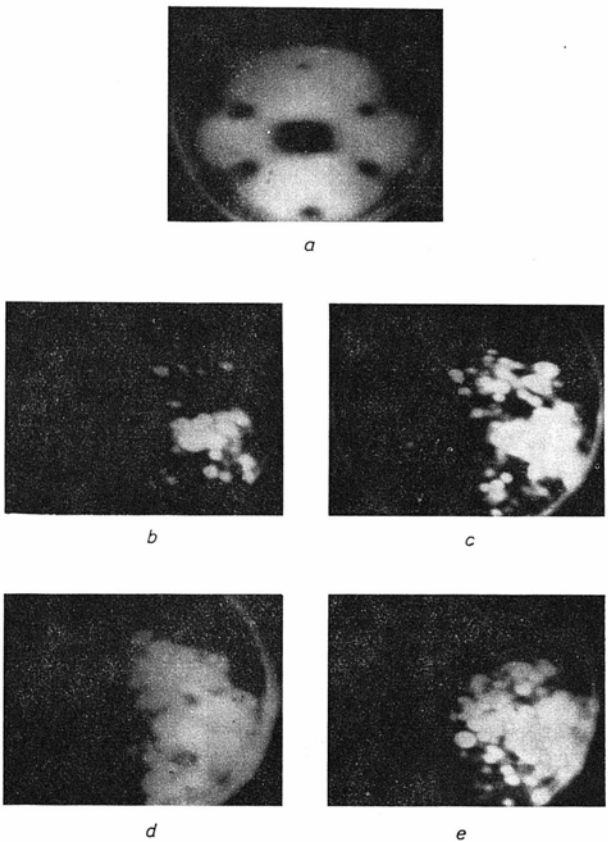

FIG. 8

Preparation of a $Pd/WO_x/W$ sample: *a* clean tungsten surface (imaging voltage $V = 6$ kV, $T = 78$ K); *b* palladium deposited from the right side, onto the oxidized tip during 15 s ($V = 8$ kV, $T = 78$ K); *c* palladium deposition continued, total deposition time 60 s ($V = 8$ kV, $T = 78$ K); *d* total deposition time 150 s ($V = 7{\cdot}5$ kV, $T = 78$ K); *e* the sample heated for approx. 1 s to about 1 200 K in absence of the field ($V = 7{\cdot}5$ kV, $T = 78$ K)

(WF's) of polycrystalline Pd and Mo layers is small and the intensity of the external electric field at these regions of the tip surface is not too much different. Thus it is impossible to follow the WFC's without application of the probe-hole technique. Alternatively, one can measure the photodensity of FEM images along the selected lines, crossing the image (Fig. 9). The absolute values of photodensities, of course, cannot be compared, however, the difference of density levels, corresponding to Pd and Mo regions on one image (see Fig. 10 "a_i") together with their distances from the minimum of the density curve (minimum transparency of the positive FEM image) (Fig. 10 "b_i") could be used for a rough estimation of WFC's caused by adsorption, surface migration etc.

Density curves A (Fig. 10) have been obtained along the line, crossing the region of "continuous" Mo and Pd layers and a relatively broad gap between them (approx. 30 nm). In this case the distance "a" (curve 1) corresponds to the contact potential difference $\Delta\varphi_{Pd-Mo} = 0{\cdot}6-1{\cdot}0$ eV (ref.[20]). In the presence of nitrogen molecules in the gas phase the WF of molybdenum increases and levels off with palladium (which does not chemisorb nitrogen molecules at room temperature leaving thus the WF of Pd – the distance "b" – unchanged, see Fig. 10). This means that $\Delta\varphi_{Mo-N} \approx \Delta\varphi_{Pd-Mo}$ in qualitative agreement with the published values $0{\cdot}5-1$ eV (refs[21,22]).

Density curves B (Fig. 10) have been obtained along the line, crossing the region of a small palladium island in closer neighbourhood of the molybdenum layer (a gap of about $1{\cdot}5-3{\cdot}0$ nm). All the distances on the tip surface have been roughly estimated from the known average tip radius as in the case of FIM. The tip radius has been obtained in FEM from the measured voltage[18], needed for obtaining the emission current of $1 \cdot 10^{-5}$ A. In contrast to the preceding case, the distance "b" changes in presence of nitrogen gas – the WF of Pd island changes – obviously because of the spill-over of nitrogen atoms from the molybdenum layer to the palladium island. The random variation of "b" might be due to the WFC's caused by adsorption–desorption phenomena on a small island (spill-over of nitrogen atoms, their recombination followed by desorption of molecules which are not held at the

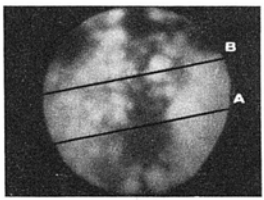

FIG. 9
Lines A and B used for densitometric measurements in Fig. 10 are shown in the FEM image of the Mo–Pd/Wo_x/W system

palladium surface at room temperature); depending on the momental state of the Pd surface during taking the photograph of a particular FEM image.

CONCLUSIONS

The presented experimental results have shown that the metal–oxide–metal (MOM) systems can be used for modeling of supported metallic and particularly bimetallic catalysts in field emission microscopes. This technique enables one to study important problems (e.g. nucleation effects, surface migration of reactants and/or of their fragments, deactivation of individual zones of the catalyst surface) in a microscopic scale. The unique feature of such studies is the direct visibility of individual components of the catalyst surface with the resolution of about 1 nm. For a particular supported bimetallic system (Pd, Mo/Wo_x) it has been proved that at room temperature molybdenum represents the trapping region for nitrogen molecules which are dissociatively chemisorbed there and afterwards, if the gap between the molybdenum

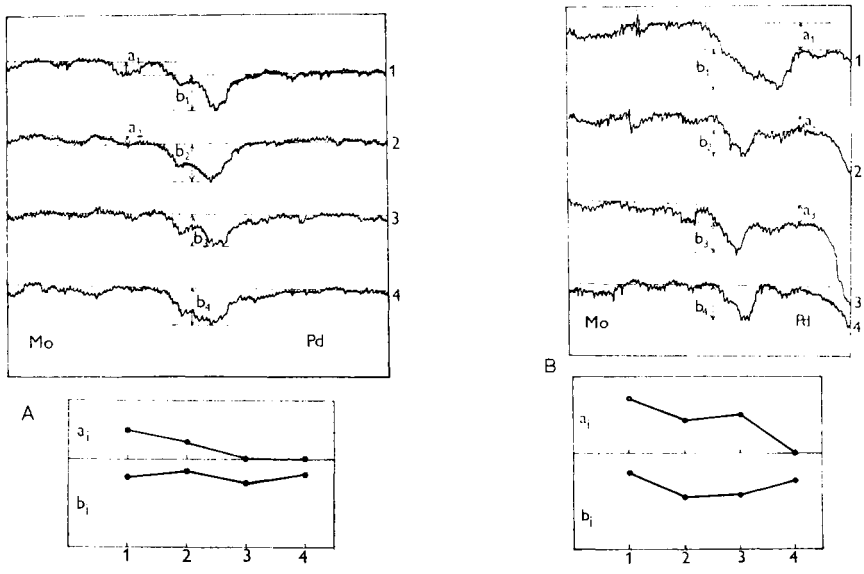

FIG. 10

Photodensity measurements on FEM images of Mo–Pd/WO_x/W system (see Fig. 9). Densitometric curves along the lines A and B (arbitrary units): 1 clean surface; 2 after the exposure of the sample 0·7 L of N_2 (at $1 \cdot 10^{-6}$ Pa) (1 L = 1 Langmuir = exposure of the sample for 1 s at $1{\cdot}33 \cdot 10^{-4}$ Pa); 3 exposure 5 L of N_2 (at the same pressure); 4 exposure 22 L of N_2 (at the same pressure). During the interaction with nitrogen the sample was held at $T \approx 300$ K

and palladium islands is of the order of magnitude of 1 nm or less a nitrogen spill-over effect can be observed.

Our experimental results thus have shown that it is possible to use field emission microscopy – a typical surface science technique, limited to a special form of samples only – for studying the problems which might be related to practical catalysis (sintering processes, poissoning of indiviual regions on the catalyst surface etc.), preserving at the same time the gnoseologic power of this technique.

REFERENCES

1. Knor Z., Kuchynka K.: Collect. Czech. Chem. Commun. *50*, 2509 (1985).
2. Knor Z., Edelmann Ch., Rudny J., Stachurski J.: Appl. Surface Sci. *25*, 107 (1986).
3. Knor Z.: Vacuum *36*, 427 (1986).
4. Gorodetskii V. V., Sobyanin V. A., Bulgakov N. N., Knor Z.: Surface Sci. *82*, 120 (1979).
5. Knor Z. in the book: *Surface and Defect Properties of Solids* (M. W. Roberts and J. M. Thomas, Eds), Vol. 6, p. 139. Chem. Soc., London 1977; Kinet. Katal. *21*, 17 (1980).
6. Knor Z.: Surface Sci. *70*, 286 (1978); in the book: *Catalysis – Science and Technology* (J. R. Anderson and M. Boudart, Eds), Vol. 3, p. 231. Springer, Berlin 1982.
7. Knor Z., in the book: *Studies in Surface Science and Catalysis, Physics of Solid Surfaces* (J. Koukal, Ed.), Vol. 23, p. 71. Elsevier, Amsterdam 1985.
8. Ozaki A., Aika K. in the book: *Catalysis – Science and Technology* (J. R. Anderson and M. Boudart, Eds.), Vol. 1, p. 87. Springer, Berlin 1981.
9. Knor Z.: Čs. Čas. Fyz., A *27*, 460 (1977).
10. Edelmann Ch. in the book: *Festkörpernalyse mit Elektronen, Ionen und Röntgenstrahlen* (O. Brümmer, J. Heydenreich, K. H. Krebs and H. G. Schneider, Eds), p. 263. VEB Deutscher Verlag der Wissenschaften, Berlin 1980.
11. Yacamán M. J., Goméz A.: Appl. Surface Sci. *19*, 348 (1984).
12. Santiesteban J., Fuentes S., Yacamán M. J.: J. Mol. Catal. *20*, 213 (1983).
13. Lewis R. T., Gomer R.: Surface Sci. *26*, 197 (1971).
14. Sugata E., Ishii S.: Surface Sci. *24*, 663 (1971).
15. Cranstoun G. K. L., Pyke D. R., Smith G. D. W.: Appl. Surface Sci. *2*, 375 (1979).
16. Cranstoun G. K. L., Anderson J. S.: Surface Sci. *32*, 397 (1972).
17. Müller E. W., Tsong T. T.: *Field Ion Microscopy*. American Elsevier, New York 1969.
18. Morin R., Drechsler M.: Surface Sci. *111*, 128 (1981).
19. Barrett Ch. S., Massalski T. B.: *Structure of Metals*. McGraw-Hill, New York 1966.
20. Hölzl J., Schulte F. K. in the book: *Solid Surface Physics. Springer Tracts in Modern Physics*, Vol. 85, p. 1. Springer, Berlin 1979.
21. Hayek K., Farnsworth H. E., Park R. L.: Surface Sci. *10*, 429 (1968).
22. Miki H., Kato K., Kawana A., Kioka T., Sugai S., Kawasaki K.: Surface Sci. *161*, 446 (1985).

Translated by the author (Z.K.).